THE ASTROPHYSICAL JOURNAL, 348:421–433, 1990 January 10

LINE PROFILES AND THE KINEMATICS OF THE NARROW-LINE REGION IN SEYFERT GALAXIES[1]

M. M. DE ROBERTIS
Department of Physics, York University, North York, Ontario, Canada

AND

RICHARD A. SHAW
Lick Observatory, University of California, Santa Cruz
Received 1989 April 11; accepted 1989 July 8

ABSTRACT

We have obtained high signal-to-noise ratio, long-slit CCD spectra at ≈ 100 km s^{-1} resolution for six high-ionization Seyfert galaxies. By subtracting the stellar absorption features with the aid of continuum templates, and using deblending techniques, we were able to measure the asymmetry indices of a number of optical emission-line profiles spanning a wide range in both ionization potential and critical density in each galaxy. These measurements are used to study the fundamental problem of the direction of cloud motion in the narrow-line region (NLR) on the assumption that the preponderance of blueward profile asymmetries requires both radial motion *and* a source of extinction. We argue by means of simple, spherically symmetric NLR simulations that infall and outflow models can be distinguished by comparing asymmetry indices as a function of ionization potential and critical density.

We confirm the positive correlation found by De Robertis and Osterbrock (at lower spectral resolution) between line width and ionization potential and/or critical density for these galaxies. We find positive correlations between the asymmetry index and both ionization potential and critical density. As well, profiles with low ionization potential and critical density have low, *but usually nonzero*, asymmetry indices. These results are most easily understood in terms of a simple NLR model in which the extinction arises primarily within radially infalling clouds; the alternative possibility of extinction arising between outflowing clouds cannot be entirely ruled out, but it is much more difficult to reconcile with these observations.

Subject headings: galaxies: internal motions — galaxies: nuclei — galaxies: Seyfert — line profiles

I. INTRODUCTION

Although much progress has been made over the past 25 years in the study of the nuclei of Seyfert galaxies, fundamental questions still abound, including the kinematics of the gas flow within a few hundred parsecs of the center of activity. Various physical models for active galactic nuclei (AGNs) have been reviewed by Osterbrock and Mathews (1986), the majority of which favor, on theoretical grounds, outflowing clouds of emission-line gas for both broad-line regions (BLRs) and narrow-line regions (NLRs). Mathews and Veilleux (1989) have also argued strongly for gas outflow, based upon stability requirements of the constituent clouds. However, a number of models have been proposed (e.g., Krolik and Vrtilek 1984; Carleton 1985; Vrtilek 1985) in which infalling gas clouds produce the emission-line spectrum.

Several lines of evidence contribute to our present understanding of the kinematics of the emission-line gas in AGNs. For example, the preponderance of blueward asymmetric, narrow emission line profiles in AGNs (e.g., Heckman *et al.* 1981; Whittle 1985*a*; Dahari and De Robertis 1988*a*, *b*) has generally been interpreted as evidence for radial cloud motion coupled with differential extinction within the NLR. That dust plays an important role in shaping the emission-line and continuum spectra in Seyfert galaxies was made abundantly clear by, for example, Dahari and De Robertis (1988*b*) and Goodrich (1989). But as Capriotti, Foltz, and Byard (1981) pointed out for BLRs, there is a twofold degeneracy in the interpretation of the blueward asymmetry: it can result either from extinction *between* radially outflowing clouds or from extinction *within* individual infalling clouds. In the first case line emission from the redshifted, outflowing clouds in the far hemisphere (as seen by the observer) suffers heavier extinction through the intercloud medium, while in the second case line emission from the illuminated faces of infalling clouds in the near hemisphere suffers heavier extinction. By itself, then, the blueward asymmetry of narrow lines provides only limited information on the kinematics of the NLR.

Recently, however, observations of low-ionization nuclear emission-line regions (LINERs) (Filippenko 1985), and Seyfert 1 and 2 galaxies (Pelat, Alloin, and Fosbury 1981; Atwood, Baldwin, and Carswell 1982; De Robertis and Osterbrock 1984, 1986; Whittle 1985*a*, *b*) have revealed that line width often correlates with critical density (N_{cr}) and/or ionization potential (IP) in AGNs. These findings strongly suggest that the NLR is stratified—that is, to first order, emission from a given ion arises in a shell-like volume surrounding the active nucleus, within clouds that are probably optically thick (in order to produce significant emission from ions with low ionization potentials). Furthermore, the dispersion velocity and number density of the clouds must decline with distance from the photoionizing continuum source. Combining these two important observations with a very simple model, it is possible to determine fundamental NLR properties like the direction of cloud motion and the distribution of dust by measuring relative asymmetries for optical emission lines spanning a wide range in critical density and ionization potential in individual

[1] *Lick Observatory Bulletin*, No. 1142.

AGNs. The resolution of this question will provide important clues to a more complete physical picture of the NLR, as well as indicate how reddening corrections should be applied to the broad-line and continuum radiation.

There are a number of important observational constraints that must be imposed in a project of this sort. In particular, we selected only high-ionization AGNs—i.e., AGNs with forbidden lines that span a broad range in IP and N_{cr}. Our sample was taken from those Seyfert galaxies studied by De Robertis and Osterbrock (1984, 1986) in which the profile full width at half-maximum (FWHM) correlates well with IP and/or N_{cr}, and where the line asymmetries were substantially different from zero. We omitted galaxies with significant Fe II emission and/or with very broad permitted lines in order to minimize the uncertainty associated with the deblending techniques used to isolate the narrow-line profiles. We used moderately high spectral resolution (≤ 2 Å) in order to minimize instrumental effects, a CCD detector with low readout noise, and a long slit in order to obtain good sky subtraction and to check whether the emission lines were spatially resolved. Our sample is composed primarily of bright galaxies in order to yield a high signal-to-noise ratio (S/N) (i.e., >30 in the continuum) in less than 1 hr exposures per spectrum. The importance of high S/N for profile analysis cannot be overstated: the discrepancy between the results of this study and those of a similar program by Appenzeller and Östreicher (1988) are due in large part, we believe, to insufficient S/N in the weaker lines in their spectra. These discrepancies will be discussed in more detail in § III. Finally, we obtained spectra of template galaxies in order to remove the effects of stellar absorption-line features which can significantly affect the asymmetry measurements for some narrow-line profiles.

II. OBSERVATIONS

We observed six program and two template galaxies at the Cassegrain focus of the Shane 3 m telescope at Lick Observatory. For these observations we used a TI 800 × 800 CCD detector on the Schmidt camera spectrograph (Lauer *et al.* 1984). Since we required high spectral resolution in order to measure the line asymmetries accurately (see § III*a*), we obtained spectra at each of four different, slightly overlapping wavelength regions using an 832 line mm^{-1} grating in second order for the bluer settings and a 1200 line mm^{-1} grating for the two redder regions. Our aim was to cover the range 3400–5100 Å and 6050–6800 Å in the rest frame of the galaxy, at or better than a resolution of 2.5 Å FWHM. Since time constraints kept us from obtaining all four spectral regions for one of our program galaxies, we supplemented the CCD data with intensified dissector-scanner (IDS) data (Robinson and Wampler 1972; Miller, Robinson, and Wampler 1976; Miller, Robinson, and Schmidt 1980) taken by D. E. Osterbrock with the same telescope and spectrograph. A journal of our observations is given in Table 1, where we list the galaxy name, the date of each observation, the wavelength range covered, the slit orientation, and the exposure time.

a) Program Galaxies

For the CCD data we observed the galaxies with a 1.″5 × 1.′2 slit to permit instrumentally limited wavelength resolution, and enough spatial coverage to ensure good sky subtraction. We extracted the spectra from bias- and flat-field–corrected CCD images by summing the signal along columns centered on the program galaxy, and subtracting the mean sky level at each channel. The mean sky level was determined by fitting a second-order polynomial to several columns which were spatially near and centered on the target spectrum, and scaling to the number of columns that were summed for the object.

Comparison spectra were recorded immediately before or after each observation of a program galaxy, and the wavelength scale was determined by fitting a third-order polynomial to the pixel positions of the comparison lines. The internal (rms) accuracy of the calibration polynomials varied from 0.02 to 0.12 Å depending primarily on the number of lines identified. The bluest scan invariably had the largest uncertainty, with only 5–8 identified lines. The absolute wavelength accuracy of these data is undoubtedly less than the internal accuracy. Judging by the formal uncertainties in the constant term of the calibration polynomials and by comparing overlapping portions of spectra taken with adjacent grating rotations, we believe that these data have an absolute accuracy of no better than 0.35 Å, or ± 25 km s^{-1}. We elected not to linearize our spectra in wavelength in order to avoid introducing interpolation errors into the line profiles. The spectra were corrected for atmospheric extinction using the mean extinction coefficients for Mount Hamilton. To determine the instrumental response, at least one, and usually two, standard stars from Stone (1977) were observed on each night. Unfortunately, the reference wavelengths of the monochromatic magnitudes for these standard stars are too far apart for more than three or four to be included within each spectrum. In order to improve the spline fit for the response curve, we used an interpolation scheme to establish additional standard flux points, taking great care to choose wavelength regions that did not include any stellar absorption features. We then adjusted our new flux points by up to 0.02 mag in such a way that the final response curve varied smoothly and slowly with wavelength. While this interpolation is obviously inferior to using measured flux points, accurate fluxing is not crucial to the success of this investigation. Osterbrock (1981) outlines the reduction procedure for the IDS observations.

b) Continuum and Emission-Line Templates

As mentioned in § I, several investigators (e.g., Filippenko 1985; Filippenko and Sargent 1985, 1987; and our own experiments) have found that emission-line profiles can be significantly affected by stellar absorption features found in AGN spectra. These absorption features come from stars in the host galaxy that are included in the spectrograph slit. Filippenko (1985) found that the stellar population often represented in AGN spectra is not unlike that from the bulges of spiral galaxies or elliptical galaxies, notably M32 (= NGC 221). This is not surprising, since most Seyferts are themselves spiral galaxies. We obtained high S/N spectra of both M32 and M31 to use as templates for the removal of stellar continuum from our program galaxies because they are bright, have closely matched stellar populations, have different central velocity dispersions, and span a fair range of metallicity, notably in CN (see, e.g., Stryker 1987).

The spectra of the template galaxies were extracted in the same way as those for the program galaxies. These spectra cover nearly the entire range between 3450 and 6940 Å in order to provide a template for the entire rest-wavelength range of interest in the program galaxies. Once the wavelength calibration polynomial was determined, however, we rebinned these spectra to a common linear wavelength scale before correcting for atmospheric extinction and placing them on a

TABLE 1

OBSERVING LOG

Object	UT Date	Wavelength Range (Å)	Slit Position	Exposure (minutes)
Mrk 1	1986 Oct 12	3454–4026	90°	60
	1986 Oct 12	4579–5403	90	40
	1986 Oct 12	6130–6937	90	40
Mrk 3	1986 Oct 12	3454–4026	0	50
	1986 Oct 11	3991–4581	180	40
	1986 Oct 11	4579–5403	180	20
	1986 Oct 11	6130–6937	180	20
Mrk 533	1986 Oct 5	3454–4026	180	60
	1986 Oct 5	3991–4581	180	60
	1986 Oct 5	4579–5403	180	30
	1986 Oct 5	6130–6937	180	30
Mrk 1073	1986 Oct 12	3454–4026	66	60
	1986 Mar 21	3991–4581	66	90
	1986 Oct 12	4579–5403	66	40
	1986 Oct 12	6130–6937	66	35
I Zw 92[a]	1987 May 6	3454–4026	90	70
	1987 May 6	3991–4581	90	70
	1987 May 6	4579–5403	90	35
	1987 May 6	6130–6937	90	45
III Zw 77	1987 May 5	3454–4026	0	90
	1987 May 6	3991–4581	90	85
	1987 May 5	4579–5403	0	45
	1988 Jul 22	6200–7380	0	60
M31[b]	1986 Oct 12	3454–4026	0	15
	1986 Oct 12	3991–4581	0	10
	1986 Oct 12	4579–5403	0	7
	1987 Nov 15	5370–6140	270	30
	1986 Oct 12	6130–6937	0	5
M32[b]	1986 Oct 12	3454–4026	90	15
	1986 Oct 12	3991–4581	90	10
	1986 Oct 12	4579–5403	90	7
	1987 Nov 15	5368–6186	270	37
	1986 Oct 12	6130–6937	90	10
NGC 7027[c]	1986 Oct 12	3454–4026	0	2
	1986 Oct 12	3991–4581	0	3.5
	1986 Oct 12	4579–5403	0	8
	1986 Oct 12	6130–6937	0	10

[a] I Zw 92 = Mrk 477.
[b] Template galaxy: see text.
[c] Line-profile standard: see text.

absolute flux scale. We then merged the spectra to form a single spectrum for the nuclei of both M31 and M32.

We noticed that the profiles of lines in our comparison spectra were slightly redward-asymmetric below the 10% relative intensity level. Although this asymmetry probably resulted from imperfect charge transfer in the CCD, and from a misalignment of the optics that direct light from the comparison lamps into the spectrograph slit, we were concerned that any instrumentally induced profile asymmetry could adversely affect our results. We evaluated the magnitude of this effect by observing the planetary nebula NGC 7027 with the same instrumental setup. The small expansion velocity ($\sim$25 km s^{-1}) of this bright, spherical nebula, combined with a $\sim$10 km s^{-1} thermal width, yields an intrinsic width of $<$30 km s^{-1}. Since this is much smaller than our 90–150 km s^{-1} instrumental resolution, we were confident that any asymmetries in the emission lines of this nebula would be a good measure of the instrumentally induced asymmetries. As we anticipated, most (but not all) of the asymmetry resulted from the comparison optics and charge transfer, and the remaining effect was too small (above the 10% intensity level) to affect the profile measurements. The profile measurements for the lines in NGC 7027, which involved the same techniques as those of the program galaxies, are described in § III*b* below.

III. DATA ANALYSIS

a) Profile Measurements

After the stellar absorption lines were removed from the continuum (see § II*b*), we measured the line widths and asymmetries at many intensity levels as well as the velocity of the line peaks and centroids for each emission line for each galaxy. Our first step toward removing these stellar absorption features was to transfer the template spectrum to the same absorption-line redshift and polynomial wavelength scale as the program galaxy by comparing the wavelengths of common

absorption features. Determining the absorption-line redshift for a Seyfert spectrum is often difficult because most of the absorption-line features commonly used for such measurements are at least partially filled in by nearby emission lines (e.g., Ca I H and K, Mg I *b*, and the H I lines). Cross-correlations with the template spectra do not yield precise results because only very limited portions of the Seyfert spectra are free of line emission. As a result, we treated the exact absorption-line redshift as a parameter that could be varied slightly to produce the smoothest residual spectrum. The redshifted template spectrum was convolved with a Gaussian function whose width was chosen such that the widths of the stellar absorption profiles in the template approximately matched those of the program galaxy. We scaled the intensity and adjusted the redshift in the template spectrum in such a way that, upon subtraction, the stellar absorption features in the program galaxies were minimized, leaving (ideally) a flat, smooth continuum. An example of the success of this technique is illustrated in Figure 1 for Mrk 3. In practice the templates were never a perfect match to the underlying stellar features, and only the emission-line profiles containing an absorption line with a relatively large equivalent width were found to be significantly affected by the subtraction procedure. Although our eye estimates of the scale factors are somewhat approximate, we found that the line profiles were not affected by these uncertainties.

Whatever the spectral resolution, the high velocities associated with mass motion in the emission-line regions can lead to blending in adjacent lines, particularly [N II] $\lambda\lambda$6548, 6583 with Hα, [O I] λ6300 with [S III] λ6312, Hγ with [O III] λ4363, [Ne III] λ3869 with Fe V λ3893, and the [S II] doublets $\lambda\lambda$4069, 4076 and $\lambda\lambda$6716, 6731. The deblending techniques employed here are much the same as described in De Robertis and Osterbrock (1984). One exception involved the [S II] doublet $\lambda\lambda$4069, 4076, which was deblended by assuming that the profiles are identical, and the ratio of the blue to the red components is 4.5 (which is appropriate for gas densities near N_{cr} for this ion). The [O II] pair $\lambda\lambda$3726.1, 3728.8 was problematic, in that the line widths are much broader than their separation. No deblending was attempted; rather, we measured the profiles as if they were one line. The measurements for this pair are therefore very uncertain and will be explicitly noted in the figures.

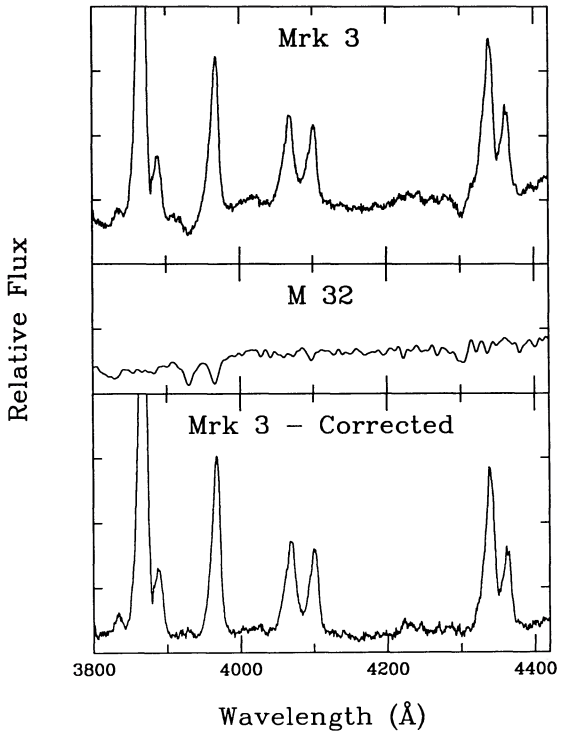

FIG. 1.—Example of the template subtraction technique used to remove stellar absorption lines from the spectrum of Mrk 3. The observed spectrum (*top*) shows the strong 3964.7 Å H line of Ca II, which skews the blue wing of the [Ne III] 3967.5 Å emission line. The H and K lines of Ca II are the strongest of many features in the template spectrum of M32 (*middle*). They are completely removed in the template-subtracted spectrum (*bottom*), restoring the profiles of the emission lines and leaving a flat continuum.

The measurements are presented in Tables 2–7 (for each galaxy separately), where we list, in order, the rest wavelength, its ionic identification, the instrumentally corrected FWHM (in km s^{-1}), and the asymmetry at the 33% and 20% intensity levels. As originally defined by Heckman *et al.* (1981), the relative asymmetry of a profile, AI, at a fraction i of its maximum intensity, is AIi = 2[$\Lambda_c - \lambda_c(i)$]/$w(i)$. Here $\lambda_c(i)$ and $w(i)$ are the line center and width at relative intensity i, respectively, and Λ_c

TABLE 2

LINE-PROFILE MEASUREMENTS FOR MARKARIAN 1

Wavelength (Å)	Identification	FWHM (km s^{-1})	AI33	AI20	v_{peak} (km s^{-1})	v_{cent} (km s^{-1})
3425.9.....	[Ne V]	584	0.13	0.19	...	...
3727.4.....	[O II]	707	0.15	0.19	4697	4633
3868.8.....	[Ne III]	633	0.14	0.18	4782	4741
4685.7.....	He II	653	0.13	0.19	4786	4715
4861.3.....	Hβ	617	0.07	0.11	4777	4748
4958.9.....	[O III]	658	...	...	4812	4787
5006.9.....	[O III]	654	0.13	0.18	4822	4773
5199.2.....	[N I]	331	0.00	0.01	4680	4666
6086.9.....	[Fe VII]	991	0.35	0.38	4774	4748
6300.3.....	[O I]	682	0.12	0.13	4817	4791
6363.8.....	[O I]	653	...	...	4816	4813
6562.8.....	Hα	532	...	...	4795	4778
6583.4.....	[N II]	561	0.13	0.15	4804	4767
6716.4.....	[S II]	492	0.07	0.07	4778	4764
6730.8.....	[S II]	482	0.02	0.09	4784	4786

TABLE 3

LINE-PROFILE MEASUREMENTS FOR MARKARIAN 3

Wavelength (Å)	Identification	FWHM (km s^{-1})	AI33	AI20	v_{peak} (km s^{-1})	v_{cent} (km s^{-1})
3425.9	[Ne v]	856	0.28	0.28	...	...
3727.4	[O II]	998	0.20	0.21	4011	3922
3868.8	[Ne III]	895	0.25	0.26	4145	4053
3967.5	[Ne III]	920	0.20	0.22	4195	4100
4068.6	[S II]	1130	0.05	0.07	4188	4109
4363.2	[O III]	899	0.18	0.16	4131	4100
4685.7	He II	894	...	...	...	3876
4861.3	Hβ	950	0.19	0.19	4078	4027
4958.9	[O III]	982	...	...	4150	4075
5006.9	[O III]	958	0.23	0.24	4167	4081
5199.2	[N I]	591	0.16	0.16	4155	4101
6086.9	[Fe VII]	1273	0.27	0.26	4120	4016
6300.3	[O I]	758	0.13	0.15	4084	4064
6562.8	Hα	908	0.16	0.17	4074	4073
6583.4	[N II]	870	0.16	0.16	4080	4062
6716.4	[S II]	674	0.03	0.06	4035	4046
6730.8	[S II]	636	0.03	0.06	4048	4079

TABLE 4

LINE-PROFILE MEASUREMENTS FOR MARKARIAN 533

Wavelength (Å)	Identification	FWHM (km s^{-1})	AI33	AI20	v_{peak} (km s^{-1})	v_{cent} (km s^{-1})
3425.9	[Ne v]	350	0.34	0.39	...	...
3727.4	[O II]	518	0.07	0.09	8714	8696
3868.8	[Ne III]	380	0.22	0.34	8759	8720
3967.5	[Ne III]	515	0.26	0.36	8749	8731
4068.6	[S II]	556	0.03	0.16	8747	8840
4363.2	[O III]	521	0.26	0.31	8718	8656
4685.7	He II	526	0.39	0.48	8710	8649
4861.3	Hβ	415	0.07	0.19	8707	8687
4958.9	[O III]	426	...	...	8751	8713
5006.9	[O III]	435	0.27	0.49	8772	8726
5199.2	[N I]	421	0.01	0.04	8888	8910
6086.9	[Fe VII]	1031	0.38	0.44	8545	8558
6300.3	[O I]	469	0.00	0.02	8773	8775
6562.8	Hα	376	0.12	0.21	8730	8711
6583.4	[N II]	377	0.04	0.07	8741	8731
6716.4	[S II]	335	−0.06	−0.10	8722	8735
6730.8	[S II]	367	−0.06	−0.10	8737	8747

TABLE 5

LINE-PROFILE MEASUREMENTS FOR MARKARIAN 1073

Wavelength (Å)	Identification	FWHM (km s^{-1})	AI33	AI20	v_{peak} (km s^{-1})	v_{cent} (km s^{-1})
3425.9	[Ne v]	339	0.13	0.19	...	...
3727.4	[O II]	514	0.04	0.09	7057	7042
3868.8	[Ne III]	261	0.04	0.14	7047	7027
4685.7	He II	391	0.14	0.21	7034	7007
4861.3	Hβ	336	0.05	0.04	7043	7028
4958.9	[O III]	317	...	...	7077	7073
5006.9	[O III]	305	0.01	0.08	7098	7088
5199.2	[N I]	326	−0.14	−0.12	7175	7223
6086.9	[Fe VII]	621	0.29	0.25	6985	6975
6300.3	[O I]	279	0.03	0.01	7084	7081
6562.8	Hα	283	...	...	7063	7043
6583.4	[N II]	262	...	0.16	7070	7049
6716.4	[S II]	204	0.00	−0.01	7083	7085
6730.8	[S II]	261	0.14	0.16	7074	7022

TABLE 6

LINE-PROFILE MEASUREMENTS FOR I ZW 92[a]

Wavelength (Å)	Identification	FWHM (km s^{-1})	AI33	AI20	v_{peak} (km s^{-1})	v_{cent} (km s^{-1})
3345.9.....	[Ne v]	572	...	...	...	...
3425.9.....	[Ne v]	461	−0.11	−0.08	...	...
3727.4.....	[O II]	468	0.04	0.08	11294	11311
3868.8.....	[Ne III]	380	−0.08	−0.02	11344	11285
3967.5.....	[Ne III]	434	0.02	0.04	11400	11405
4068.6.....	[S II]	390	−0.05	0.01	11306	11327
4363.2.....	[O III]	463	−0.07	0.00	11280	11315
4685.7.....	He II	428	0.00	0.03	11295	11298
4861.3.....	Hβ	329	−0.04	0.00	11333	11336
4958.9.....	[O III]	388	...	...	11317	11315
5006.9.....	[O III]	473	0.10	0.14	11326	11314
6086.9.....	[Fe VII]	583	−0.04	0.13	11338	11401
6300.3.....	[O I]	322	−0.06	0.01	11331	11333
6562.8.....	Hα	296	0.01	0.02	11326	11327
6583.4.....	[N II]	278	0.05	0.07	11315	11311

[a] I Zw 92 = Mrk 477.

is the wavelength of the peak of the profile as defined by a second-order fit to the central 3–5 data points. The last two columns list the radial velocity ($c\Delta\lambda/\lambda_0$) of the line peak and of the entire profile centroid, respectively.

We confirm the earlier correlations between line width and both IP and N_{cr} found by De Robertis and Osterbrock (1986). Some of the correlations are marginally better, since we have higher resolution and higher S/N data. (Note that widths for [O II] λ3727 are too large because of the partial blending of these lines.) We also examined our program galaxies for spatial profile variations along the slit. While we found none at a spatial resolution of ∼1″.5 along the position angles listed in Table 1, we were concerned with the spatial variations found by Whittle *et al.* (1988), who investigated [O III] λ5007 substructure (at higher wavelength and similar spatial resolution) in connection with radio lobes that are seen in some Seyfert galaxies. Such substructure, which may result from shocked gas and/or star formation activity near the nucleus, would confuse the analysis presented here. While Whittle *et al.* (1988) found significant [O III] profile variations along the radio axis in Mrk 3, their slit was oriented nearly perpendicular to ours (see Table 1). They found less extended emission, and smaller profile variation (with no narrow off-nuclear component), along position angle 175°, so that the absence of spatial variation along our slit is not surprising.

Similarly, other studies (e.g., Veilleux 1989) at very high dispersion reveal velocity substructure in many (but not all) emission lines in some Seyfert galaxies, notably Mrk 533 and Mrk 1073. Whether these features result from extinction within or emission from single clouds or cloud complexes is unclear, but the unresolved substructure is usually superposed upon an otherwise smooth, but blueward-asymmetric, profile. If the effects are no larger in the other program galaxies, then we expect that the correlations (presented in § III*b*) between profile asymmetry and other parameters will still be valid, albeit with increased scatter. We remain confident that, on average, both the ionization and the number density in the NLR clouds decrease outward from the center of all the Seyfert galaxies in this study.

b) Profile Analysis

We plot the line asymmetry at the 20% level (AI20) against both IP and N_{cr} in Figures 2 and 3. The collisionally excited lines are indicated by solid symbols, and the recombination

TABLE 7

LINE-PROFILE MEASUREMENTS FOR III ZW 77

Wavelength (Å)	Identification	FWHM (km s^{-1})	AI33	AI20	v_{peak} (km s^{-1})	v_{cent} (km s^{-1})
3345.8.....	[Ne v]	428	0.12	0.15	...	...
3425.9.....	[Ne v]	342	0.02	0.02	...	...
3587.8.....	[Fe VII]	362	0.06	0.05	10082	10090
3727.4.....	[O II]	461	0.03	0.10	10135	10150
3760.3.....	[Fe VII]	330	0.15	0.19	10058	10041
3868.8.....	[Ne III]	264	0.08	0.09	10140	10121
3967.5.....	[Ne III]	427	0.12	0.07	10180	10216
4363.2.....	[O III]	271	0.04	0.00	10147	10138
4685.7.....	He II	359	−0.01	−0.02	10147	10160
4861.3.....	Hβ	...	...	0.19	10158	...
4958.9.....	[O III]	283	...	...	10152	10132
5006.9.....	[O III]	301	0.11	0.13	10153	10128
6086.9.....	[Fe VII]	390	0.15	0.09	10232	10205
6374.5.....	[Fe X]	305	0.13	0.09	10205	10211

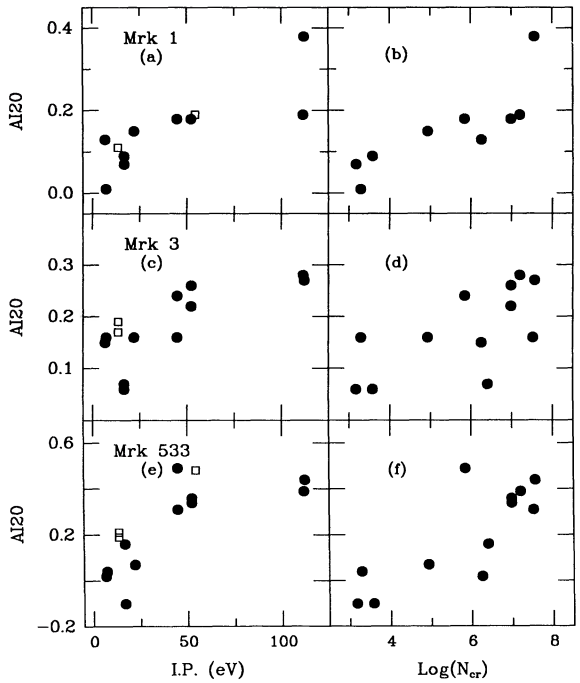

FIG. 2.—Plots of mean IP and log N_{cr} vs. line asymmetry, AI20, for Mrk 1 (*a*, *b*), Mrk 3 (*c*, *d*), and Mrk 533 (*e*, *f*). Open circles indicate less certain [O II] λ3727 results (see text), and open squares denote H and He recombination lines.

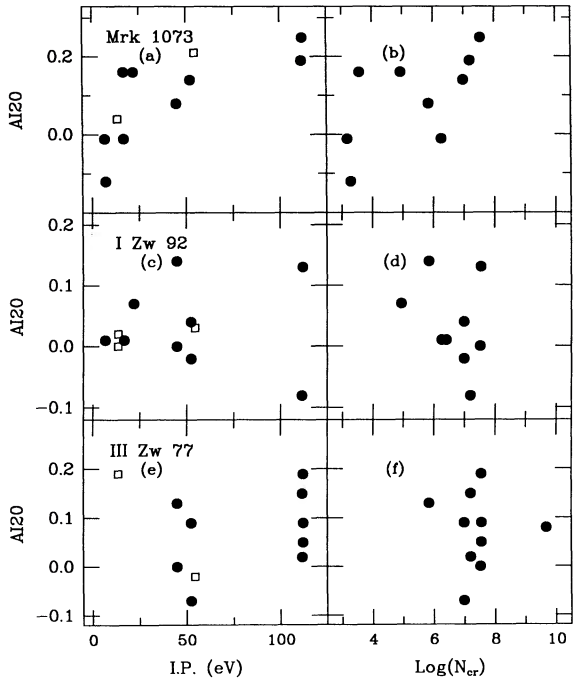

FIG. 3.—Same as Fig. 2, but for Mrk 1073 (*a*, *b*), I Zw 92 (*c*, *d*), and III Zw 77 (*e*, *f*).

lines of H I and He II (in the IP plots only) with open symbols. As in De Robertis and Osterbrock (1986), we plot the mean IP, meaning the average between the energy required to produce that ion and the next higher state. Most of the galaxies show fair to good positive correlations between asymmetry and both IP and N_{cr}—i.e., as IP or N_{cr} increases, so does AI20. (There seems to be little, if any, trend for I Zw 92 and III Zw 77, but we were unable to measure the lowest ionization lines in the latter.) Notice that the low-ionization (or critical density) lines have small, *but usually nonzero*, asymmetries. Furthermore, the high–IP lines generally have higher asymmetries *at all levels* than the low–IP lines, as Figure 4 illustrates for Mrk 1. Finally, we find some indication that lines with the highest IP and/or N_{cr} also have the smallest radial velocities, and vice versa, whether measured from the line peak or the centroid, but the correlations (not shown) are fairly weak. Although the zero-point errors in our spectra were estimated to be ~ 25 km s^{-1} (see § II*a*)—much less than the range of values measured for each object—they could nevertheless reduce the significance of the correlation. We note that the weak velocity correlations persist even when only the red spectrum (containing [Fe VII], [Fe X], [O I], [N II], and [S II]) is used, where the uncertainty is dominated by the smaller internal errors.

If the profile asymmetries are indeed caused by the combined effects of differential extinction and radial cloud motion, then the above results show that the highest IP and N_{cr} lines, which are formed near the center of activity, suffer the greatest extinction, and vice versa. The most straightforward interpretation is that most of the dust is confined to the NLR clouds themselves, which we might expect if the gas-to-dust ratio within the NLR is constant. If that is the case, then, following the discussion in § I, the clouds must be radially infalling in order to produce the observed blueward-asymmetric profiles. We note that while these observations do not preclude the possibility of outflow, most of the dust must in that case be distributed between the clouds in a nonuniform way.

We note a discrepancy between the results obtained here and those of Appenzeller and Östreicher (1988), who stated that while the lower ionization lines in their high-dispersion spectra showed distinct profile asymmetries, they found the higher ionization lines to be more symmetric, or nearly Gaussian, in profile. Oddly, they do not include the "extended low-

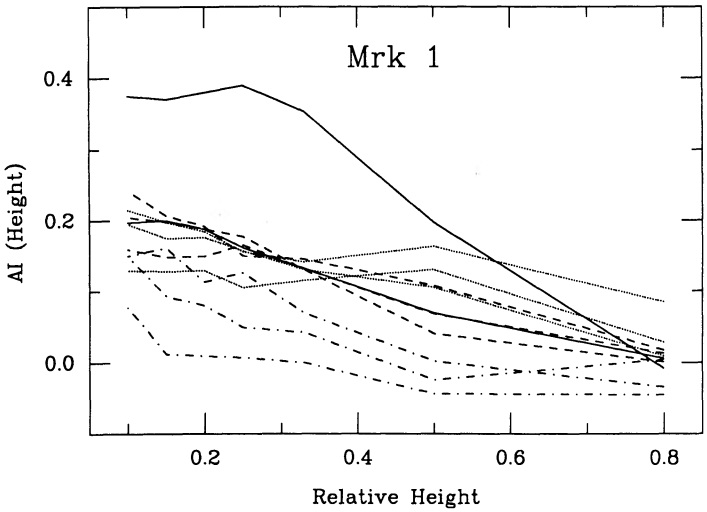

FIG. 4.—Measured line asymmetry as a function of relative line height for Mrk 1. The curves are grouped roughly according to IP and/or N_{cr}. *Solid lines*: [Ne V] λ3426, [Fe VII] λ6087; *dotted lines*: [Ne III] λ3869, [O III] λ5007, [O I] λ6300; *dashed lines*: [O II] λ3727, He II λ4686, [N II] λ6584; *dot-dash lines*: H I λ4861, [N I] λ5200, [S II] λ6731.

intensity wings" in their evaluation of the high-ionization line profiles, which is where most of the effect of differential extinction would occur. Unfortunately, the S/N in their spectra is rather low (for this sort of analysis), and their profiles are all the more uncertain because no correction was made for contaminating continuum features such as Fe II, broad Balmer lines, and stellar absorption lines. Still, their figures suggest to us that, with a more detailed analysis, Appenzeller and Östreicher's data may not conflict with ours at all.

IV. MODELS

In order to demonstrate the potential for asymmetry observations to probe conditions in the NLR, we now present simple, spherically symmetric models of the NLR. We consider only the two limiting cases that are consistent with blueward asymmetric profiles: one in which the extinction is confined completely to the medium between outflowing emission-line clouds and the other in which the extinction arises entirely within infalling emission-line clouds. Although one might question whether conditions hypothesized for the intercloud medium (e.g., Krolik and Vrtilek 1984) permit the survival of dust (which probably causes the reddening and profile asymmetries; see, e.g., Dahari and De Robertis 1988*a*, *b*), simple sputtering calculations suggest that dust may in fact survive for a significant fraction of the NLR crossing time.

The objective of the following exercise is not to present a complete physical model for the NLR, but rather to describe a method for generating realistic profiles (i.e., profiles that resemble those we observe at ~ 1 Å resolution) in order to study qualitatively how they are affected by various distributions of attenuating material. In each case we must compare the line profiles generated by our model for the outer NLR, where only lower ionization lines are formed, with the inner NLR where the higher ionization lines are produced. We modeled each region of the NLR by uniformly filling a spherical shell between inner and outer radii R_i and R_o with N_c discrete emission-line clouds. The origin of coordinates corresponds to the nonthermal continuum source, i.e., the center of the NLR. For each cloud, a radial velocity was selected randomly from a Gaussian distribution with a mean of $V_0 = 325$ km s^{-1} and a dispersion $\sigma = 250$ km s^{-1}, yielding profiles that closely resemble those observed. Every experiment was performed using 25,000 clouds, but the resulting line profiles were not sensitive to this choice as long as the number was large enough to generate a smooth profile. The contributions to the emission from the individual clouds were weighted by the appropriate absorption law, convolved with a Gaussian instrumental profile (FWHM = 90 km s^{-1}), and then summed to yield the calculated profile. The widths and asymmetries were then measured in the same way as for the observed profiles, except that the measurements were performed in velocity space. For the inner NLR, the radial boundaries were chosen to be a factor of 10 smaller than the outer NLR, while all the other parameters remained the same. Note that, for all models, reversing the direction of cloud motion is equivalent to reflecting the profile about the zero-velocity axis.

We note here that the line asymmetries derived from these calculations are quite insensitive both to our choice of the mean and dispersion velocities in the Gaussian distribution (as long as they were of this order) and to the ratio R_o/R_i. Since we assume that the line widths decrease with distance from the ionizing continuum source, our choice of a constant mean and dispersion velocities for our models of both the inner and the outer NLR might at first glance seem inappropriate, if not contradictory. The crucial point here is that the asymmetry index is *normalized to the line width* (see § III), so that scaling the profiles in velocity space is an irrelevant complication for our purpose. In fact, we have verified this conclusion by explicit calculation using very different values for the velocity parameters for the inner and outer regions, and the results are qualitatively identical and quantitatively similar. In fact, the precise form of the velocity law turns out not to matter either: a purely triangular velocity distribution, for example, produces the same qualitative results. Our interpretation mainly requires that the emission-line region be spherically symmetric—i.e., that line asymmetry results from radial motion and attenuation and not from the spatial distribution of the clouds. Indeed, apart from velocity scaling, narrow-line profiles representing different ionization potentials critical densities are rather similar for a given object (e.g., De Robertis and Osterbrock 1984; Whittle 1985*b*), which implies a single underlying acceleration mechanism and geometry for the NLR.

a) Outflow

For the case of outflow, the entire NLR (from 0 to R_o) was filled with attenuating material according to either a uniform, $1/r$, or a $1/r^2$ density law with the restriction that the total mass of dust in the NLR be constant. The total extinction (in magnitudes) along the observer's line of sight through the symmetry axis, Δm, is the parameter of interest here, and is clearly an upper limit to the attenuation observed in a real nucleus. (Actually, Δm is an exact measure of the maximum extinction only for the uniform density case. For nonuniform density laws, Δm represents the attenuation averaged over a small solid angle about the symmetry axis.) The effective optical depth along the line of sight depends upon the density distribution and path length through the NLR. Figure 5 shows an example for the outer NLR in which uniform, $1/r$, and $1/r^2$ dust distributions, respectively, were used. The different curves illustrate both the absolute and the relative effects of varying the total extinction in the NLR. The maximum extinction (expressed in magnitudes) and corresponding relative asymmetries are provided in the legend in each panel. Evidently, in order to generate AI20's comparable to those observed in the outer NLR, a dust distribution that is not centrally condensed is required. Figure 6 illustrates the same experiment using the same density distributions, but this time for the inner NLR. In this case the distribution *must* be centrally condensed to generate large asymmetries. Thus, it is apparently not possible to satisfy the observational constraints for both the low and the high critical density emission-line profiles simultaneously in these models. We view this as a serious flaw for the outflow interpretation, although, as noted above, a more complex geometry involving outflow might be reconciled with our observations.

The line-profile parameters measured for the outflow models for the outer and inner NLR are presented in Tables 8 and 9, respectively. For each value of the maximum extinction we measured the differences between the rest velocity and that of both the peak and centroid of the profile, $\Delta v_{\rm peak}$ and $\Delta v_{\rm cent}$, respectively. (These differences measure the apparent blueshift of the profile relative to the systemic velocity of the nucleus.) We also list the FWHM and AI20 in the following columns. In all cases, large relative asymmetries accompany higher differential extinction, larger apparent blueshifts, and (usually)

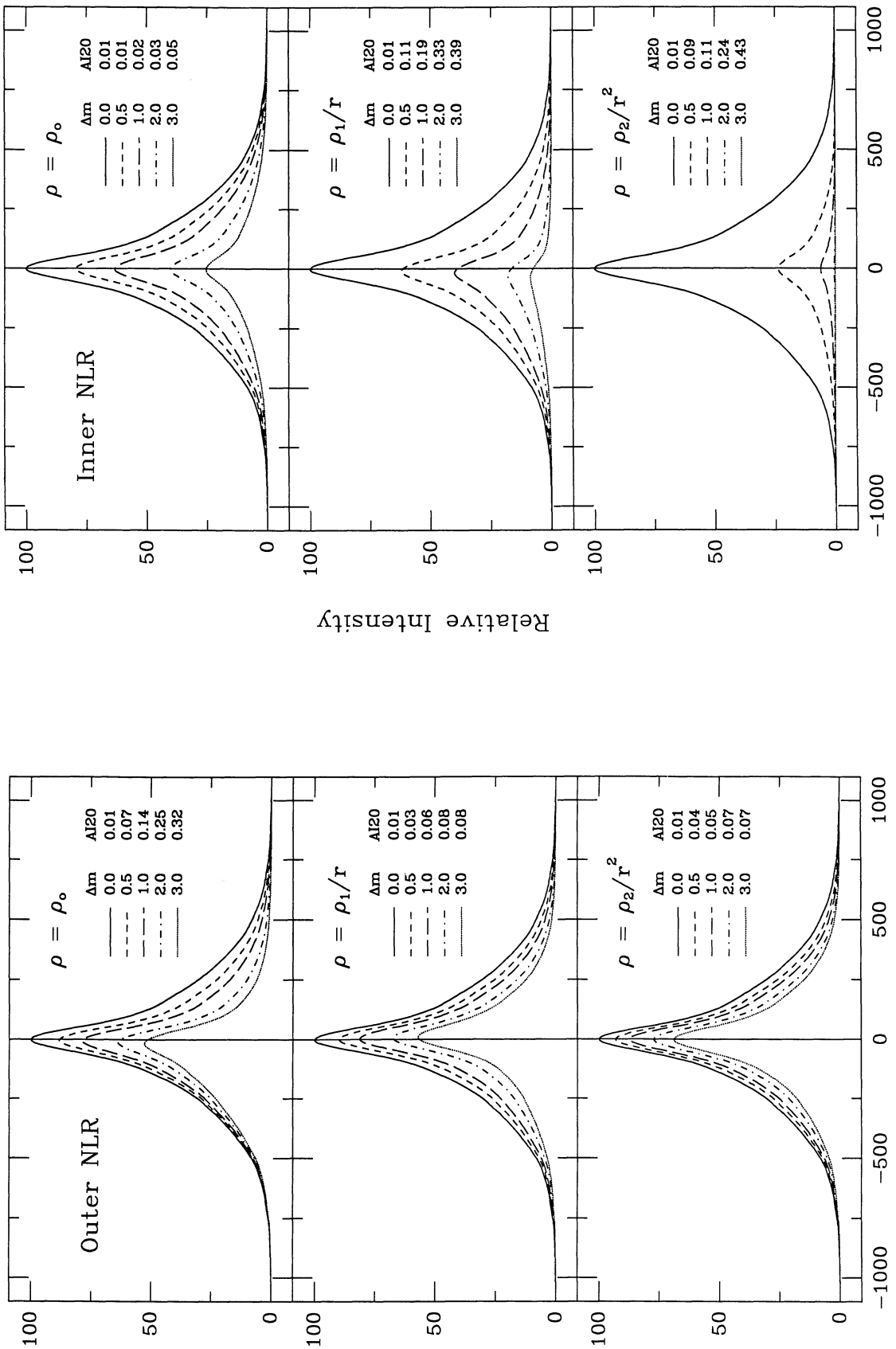

FIG. 5

FIG. 6

FIG. 5.—Line profiles for outer NLR for outflow models described in text. Maximum extinction (Δm) and asymmetry parameter (AI20) are listed in the legend for each model.

FIG. 6.—Same as Fig. 5, but for inner NLR for outflow models described in text

TABLE 8

OUTFLOW MODEL PARAMETERS: OUTER NLR

Extinction (mag)	Δv_{peak} (km s^{-1})	Δv_{cent} (km s^{-1})	FWHM (km s^{-1})	AI20
A. Uniform Dust Distribution				
0.0.....	1.2	1.8	273	0.006
0.5.....	4.2	16.8	267	0.074
1.0.....	7.2	30.5	266	0.141
2.0.....	12.0	55.1	274	0.247
3.0.....	16.2	76.0	287	0.323
5.0.....	25.1	107.2	314	0.395
B. $1/r$ Dust Distribution				
0.0.....	1.2	1.8	273	0.006
0.5.....	0.0	4.2	261	0.034
1.0.....	−1.8	4.8	250	0.055
2.0.....	−5.3	3.0	232	0.081
3.0.....	−6.9	0.0	216	0.083
C. $1/r^2$ Dust Distribution				
0.0.....	1.2	1.8	273	0.006
0.5.....	1.7	7.2	261	0.035
1.0.....	1.8	9.6	252	0.051
2.0.....	1.8	12.0	240	0.066
3.0.....	1.8	13.2	230	0.071

broader profiles. An estimate of the numerical uncertainties resulting from this artificial profile generation process can be made from the zero-extinction models where the profile shifts and asymmetries are not exactly zero. It is interesting to note that the line widths derived from the models decrease for the outer NLR with centrally concentrated dust distributions. This is because emission in the line core (which comes from a region perpendicular to the line of sight) is slightly enhanced compared with emission in the wings of the line. For the inner NLR, this happens only for the most concentrated distribution.

TABLE 9

OUTFLOW MODEL PARAMETERS: INNER NLR

Extinction (mag)	Δv_{peak} (km s^{-1})	Δ_{cent} (km s^{-1})	FWHM (km s^{-1})	AI20
A. Uniform Dust Distribution				
0.0.....	1.2	1.8	273	0.006
0.5.....	1.8	3.6	274	0.012
1.0.....	2.0	4.8	274	0.019
2.0.....	2.4	8.4	274	0.032
3.0.....	3.0	11.4	274	0.046
5.0.....	4.2	17.4	276	0.074
B. $1/r$ Dust Distribution				
0.0.....	1.2	1.8	273	0.006
0.5.....	9.6	30.5	270	0.107
1.0.....	17.4	55.1	275	0.194
2.0.....	31.1	92.8	285	0.330
3.0.....	40.1	115.0	294	0.392
C. $1/r^2$ Dust Distribution				
0.0.....	1.2	1.8	273	0.006
0.5.....	1.8	15.6	225	0.089
1.0.....	2.4	19.8	207	0.114
2.0.....	3.0	34.1	192	0.244
3.0.....	4.2	68.3	194	0.432

b) Inflow

We find that simple inflow models, where the dust is confined to the clouds, are consistent with the observations for reasonable assumptions. The only difference in the treatment between this model and those discussed above is that in this model the amount of attenuation is a function not of the path length through the NLR but rather of the path length through the individual emitting clouds along the line of sight. (We assume that shadowing effects are not important, i.e., the emission is not further attenuated in the NLR after passing through the cloud in which it was generated.) In effect, an extra parameter has to be introduced with inflow models that describes the geometry of the clouds. Unfortunately, the need to introduce this parameterization prohibits a more quantitative study of the cloud distribution in the NLR with this model. The qualitative behavior of all of our models is consistent, however. Reasonable profiles can be produced with inflowing clouds, and larger asymmetries are found for higher critical density lines, *if* the gas-to-dust ratios in the emission-line clouds is not substantially different throughout the NLR *and if* the effective column density increases with number density. The latter is not an unreasonable hypothesis, for if the mass function of clouds is independent of position in the NLR, then the requirement that the clouds be in pressure equilibrium with the ambient medium would mean that they are compressed as they approach the center, leading to higher number densities. Higher column densities (and higher extinction optical depths) would follow if the clouds maintained any semblance of their previous low-density shape. We note that the distinction between the outer and inner NLR in this instance arises naturally because larger column densities near the center lead to larger asymmetries without reference to a specific cloud shape. If, however, the clouds remain self-similar throughout the NLR, then it can be shown that the optical depth through the clouds is proportional to the cloud number density to the two-thirds power. (Pressure equilibrium between the clouds and the intercloud medium ensures that the intercloud medium pressure is proportional to the cloud number density.) As a result, the pressure in the intercloud medium varies as the optical depth to the four-thirds power. Observational constraints on inflow models seem to suggest that the optical depth may vary by approximately 5 from the outer to the inner NLR clouds. Thus, we would expect the intercloud medium pressure to vary by ~ 8 between the [O III] and the [S II] regions, for example. This is an order of magnitude less than estimates based on critical density arguments (e.g., De Robertis and Osterbrock 1986) and may be an indication that the clouds do vary in shape in the NLR.

To illustrate profiles generated according to the inflow model, we assume that the clouds are quasi-spherical with an optical depth proportional to $(1 + \cos \theta)^n$, where θ is the angle made by the cloud to the line of sight along the symmetry axis and $n \sim 1$. The left-hand and right-hand panels of Figure 7 show inflow models with various degrees of total extinction for cases $n = 1$ and $n = 2$, respectively. The line profiles and asymmetries are not unlike those observed in our program galaxies. Table 10 presents the relevant model parameters for the inflow models for the two values of n. In each case, the magnitude of extinction, profile blueshift, line width, and asymmetry index all increase for low to moderate values of the extinction. The asymmetry index appears to decrease for very large values of extinction because the profile itself begins to lose its character-

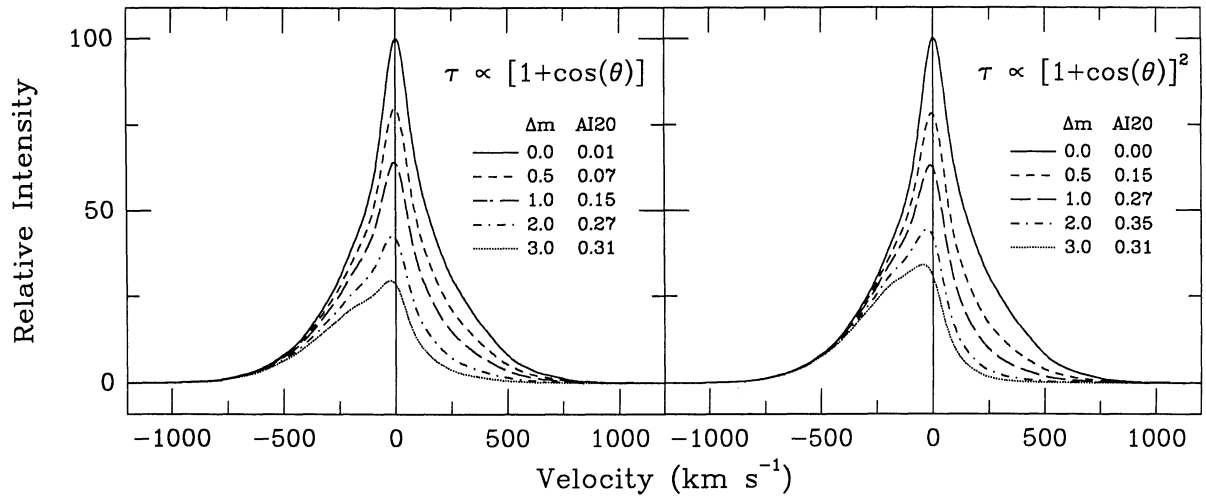

FIG. 7.—Same as Fig. 5, but for inflow models described in text. Only one region was computed for this case, since the inner and outer regions differ only in the amount of intracloud extinction.

istic shape, showing secondary maxima. Adding more clouds helps somewhat, but it would appear that the differential extinction in the NLR is constrained to be less than ~3 mag.

V. DISCUSSION AND SUMMARY

Before we review the implications of our models, it is perhaps worth recounting the observational results and interpretations (see references in § I) that lead to our physical picture of the NLR. First, we note that narrow emission lines in most Seyfert galaxies are quite symmetric, and that when they are asymmetric it is usually to the blue—i.e., the blue wing is stronger than the red wing. Second, we adopt the interpretation that the asymmetries usually, if not always, result from a combination of extinction and radial motion of the clouds that produce the narrow lines. Third, the correlations found for many Seyfert galaxies between line width and both IP and N_{cr} imply a NLR in which dispersion velocity, ionization, and cloud density all decline, on average, with distance from the central source of ionizing continuum. Fourth, we have found that the line asymmetry declines with IP and N_{cr} and, as our models (see § IV) show, this is most easily interpreted in terms of radially infalling narrow-line clouds which contain most of the attenuating material in the NLR. We present below some additional arguments that must be considered in a discussion of the direction of gas flow in the NLR of AGNs.

TABLE 10

INFLOW MODEL PARAMETERS

Extinction (mag)	Δv_{peak} (km s^{-1})	Δv_{cent} (km s^{-1})	FWHM (km s^{-1})	AI20
A. $\tau \propto (1 + \cos\theta)^1$				
0.0	−1.2	−1.8	273	−0.005
0.5	2.4	16.8	280	0.074
1.0	6.0	35.9	299	0.151
2.0	13.8	76.6	344	0.268
3.0	24.0	116.2	398	0.310
5.0	66.5	177.2	476	0.231
B. $\tau \propto (1 + \cos\theta)^2$				
0.0	−1.2	−1.8	273	−0.005
0.5	5.4	32.9	279	0.154
1.0	12.0	64.1	304	0.266
2.0	26.3	115.0	357	0.352
3.0	44.9	148.5	399	0.311
5.0	116.7	187.4	437	0.254

The chief virtue of the infall model is its simplicity: it can qualitatively reproduce observations of the relative asymmetries in both high- and low-ionization emission lines despite the fact that the cloud structure and distribution of dust within the clouds remain uncertain. In some sense, the infall model presents a simpler picture than the outflow model because an accretion flow is already hypothesized to fuel the central supermassive object according to the standard model. Outflow models have the added difficulty of driving large quantities of gas from the nucleus through mechanical and radiation pressure. In the infall model, gravity would ultimately be responsible for the line widths. And yet if gas is flowing into the nucleus from distances $\gg 100$ pc, it must do so dissipatively so as to lose a great deal of angular momentum. It is not clear what mechanisms might be responsible for this process (see, however, Lin, Pringle, and Rees 1988). The infall model does not simplify the problems associated with cloud stability in the presence of a hot, rarefied intercloud medium that presumably is moving radially outward.

It is possible, of course, to generate blueward-asymmetric line profiles from either a non–spherically symmetric NLR, or from a planar or disklike distribution of dust within a spherically symmetric NLR (e.g., Osterbrock 1988). But for a planar distribution of dust, the degree of asymmetry of the emission lines would depend only upon the amount of dust and the orientation of that plane with respect to the observer, and *not* upon IP or N_{cr} as our observations would indicate. If the dust is confined to a disk with a thickness that is comparable to or larger than the outer NLR (~100 pc), then the resulting line asymmetries would increase with distance from the center (as with our outflow model), which again runs counter to our observations. It is possible to generate blueward asymmetries that increase with IP and N_{cr} (i.e., that decrease with distance from the center, but not necessarily to zero) for the case of outflow if the dust is confined to a plane which is larger than the inner boundary of the NLR (~1 pc) but smaller than the outer boundary. In this case emission from the inner region will encounter a large differential extinction, whereas emission from the outer region may or may not be asymmetric, depend-

ing upon whether the plane of dust is oriented face-on or edge-on with respect to the observer. Although this picture cannot be ruled out on the basis of our results, we believe the geometry to be rather contrived, and we are in any case unconvinced that the combination of viewing angle and dust-disk height will nearly always result in either vanishingly small asymmetries, or will produce blueward asymmetries that increase with IP and N_{cr}. Finally, the narrow-line profiles in Seyfert galaxies studied at very high wavelength resolution by Vrtilek and Carleton (1985) and Veilleux (1989) almost always have a single primary maximum, which strongly suggests that the NLR does not deviate radically from spherical symmetry. As a result, it would be difficult to reconcile these observations with a nearly planar NLR model employing either inflow or outflow. Still, moderate deviations from spherical symmetry could be important.

As noted in § IV, the presence of attenuating material in both inflow and outflow models generates apparent blueshifts in the position of the peak and centroid of an emission line relative to the velocity of the center of the host galaxy; higher ionization lines will show larger blueshifts. However, at least for the models considered here, it does not seem that blueshifts generated solely by differential extinction can explain shifts of the order of several hundred kilometres per second measured for some AGNs and QSOs (e.g., Gaskell 1982). On the other hand, most narrow emission lines in Seyfert galaxies show *no* substantial blueshift or asymmetry at ~ 100 km s^{-1} resolution. The sample studied here was selected partly on the basis that these galaxies were known to have large, blueward asymmetries. We believe this tendency of Seyferts to have symmetric narrow lines provides another strong, though indirect, argument in favor of dust being largely confined to the NLR clouds. The reason is simple: if the attenuating dust is distributed between the clouds, then Table 10 shows that the total extinction in the NLR must be significantly less than 0.5 mag, independent of the radial distribution of the dust, in order for the observed AI20's to be less than about 0.05 in both the low-and the high-ionization lines. Such a small total extinction places an upper limit on the observed Hα/Hβ ratio (narrow component) of about 3.8, which is rather low for most NLRs in AGNs (Dahari and De Robertis 1988*a*). In other words, if the dust resides primarily between the clouds, the large observed Balmer decrements are inconsistent with the small observed asymmetries in the narrow emission lines. One cannot argue that a substantial part of the larger observed extinction arises within the host disk galaxy (but outside the NLR), since the measured Balmer decrements do not correlate well with the orientation of the host galaxy (Dahari and De Robertis 1988*a*). The small upper limit to the extinction would also imply an extremely large gas-to-dust ratio in the NLR, which we believe is unlikely. Finally, there is the interesting possibility that comparable column densities of dust are present in both the NLR clouds and the ambient medium. In this way, a very large Balmer decrement could accompany small relative profile asymmetries—a consequence of the nature of integrated and differential quantities, respectively. That the column densities should be so nearly equal in most Seyferts seems highly contrived and therefore implausible. It is much more likely that one component dominates.

If the dust is largely confined to the NLR clouds, however, we encounter no inconsistency between the observed reddening and asymmetries. As Table 10 and Figure 7 show, only a modest extinction within each cloud is required to generate a substantial integrated asymmetry. Although we have not specified any size or shape for the clouds used in our inflow model, small globules within H II regions in our Galaxy have very high internal extinctions indeed. Thus, inflowing clouds with more ordinary gas-to-dust ratios provide perhaps the simplest and most consistent picture of gas flow and dust distribution within the NLR. Finally, it has always been unclear whether the nonthermal continuum radiation in AGNs should be corrected for the extinction derived from emission-line ratios. If the dust is largely confined to the clouds, however, then a substantial reddening correction should not be applied to the continuum radiation. On the other hand, the extinction as determined from the narrow-line Balmer decrement might appropriately, though not precisely, be applied to an analysis of the other narrow lines.

A small percentage of AGNs exhibit small redward asymmetries (see, e.g., De Robertis and Osterbrock 1984; Whittle 1985*b*; Dahari and De Robertis 1988*a*, *b*). If these asymmetries cannot be attributed to instrumental effects, they may result from extended emission from sites of star formation in the nucleus or from optical line emission associated with structures seen in radio maps (e.g., Whittle *et al.* 1988). This extra component might not contribute symmetrically to the profile, thereby distorting a small intrinsic blueward asymmetry by enhancing either the blue or red wing. Thus, profiles could appear symmetric or even redward-asymmetric to the observer. If the redward asymmetry cannot be explained by aperture or instrumental effects, then some or all of the following might be considered: (1) the NLR is small enough for gravitational redshifts to become important, (2) outflow is more important than inflow in some objects, (3) the mass in emission-line material is not evenly distributed between the two hemispheres. Only the first is unlikely, given the scale size of the NLR based on profile variation arguments (De Robertis 1987). In a steady state the third possibility is unlikely as well because of the large numbers of emission-line clouds postulated to exist in the NLR to explain the integrated line fluxes and to generate the smooth profiles noted even at very high resolution (Vrtilek and Carleton 1985; Veilleux 1989). But in a non–steady state situation (e.g., an ongoing merger or the accretion of a dwarf companion), material may be temporarily distributed asymmetrically, thereby leading to either redward or blueward profile asymmetries.

The Balmer decrement measured as a function of velocity could in principle be used to obtain complementary information about the NLR, since relative profile asymmetries arise through differential extinction in the NLR. The Balmer decrement measures the integrated, extinction-weighted intensity at a particular velocity, however. Significant Balmer emission would not be expected from clouds with a large neutral component, so one probably cannot probe the extremes of the NLR with this technique. To apply the Balmer decrement method in practice, one requires accurate Hα and Hβ profiles—i.e., with [N II] $\lambda\lambda$6548, 6583 removed, a correction for stellar Balmer absorption applied, and an accurate continuum level identified. While these are problems common to all line-profile analyses, they are more acute with this approach.

Observations by Antonucci and Miller (1985) and Miller and Goodrich (1987) have led some investigators (e.g., Krolik and Begelman 1988) to postulate the existence of tori in the nuclei of active galaxies. The primary role of a torus is, in the case of Seyfert 2 galaxies, to occult the BLR and nonthermal continuum source from certain lines of sight. For our purposes,

the torus would comprise a third component, possibly complicating the interpretation of our observations (as would the introduction of beams or jets along the symmetry axis of the central engine). While the torus could affect the narrow-line profiles in principle, its influence is probably not significant, since the scale size of the torus is of the same order as the BLR and the scale size of the NLR is orders of magnitude larger. We would therefore expect it to have little effect on the NLR, except perhaps for the highest ionization lines. Nevertheless, more detailed line-profile investigations should consider the effects of a torus explicitly.

In summary, it appears that simple models of the NLR in which attenuating dust is confined to radially infalling emission-line clouds are more easily able to explain the observed run of asymmetry with both IP and N_{cr} (i.e., radius), as well as the lack of narrow-line asymmetry in most AGNs with large narrow-line Balmer decrements. The alternative explanation of extinction arising between radially outflowing clouds cannot be entirely ruled out, but it would require at least a more complicated NLR geometry, and probably an extremely high gas-to-dust ratio. With the direction of motion and the general distribution of dust at least tentatively identified, it should now be possible to construct improved NLR models and so carry out a more precise investigation of the gas kinematics of the NLR.

This research was supported by NSF grant AST 86-11457 to the University of California, under the direction of D. E. Osterbrock, and by the National Sciences and Engineering Research Council of Canada (M. M. D. R.). We thank D. E. Osterbrock, W. G. Mathews, and S. Veilleux for helpful discussions and comments on the text. Support for the Lick Observatory computer hardware and data reduction software was provided through NSF grant AST 86-14510. Some additional support was provided for one of us (R. A. S) through NASA grant 5-28749.

REFERENCES

Antonucci, R. R. J., and Miller, J. S. 1985, *Ap. J.*, **297**, 621.
Appenzeller, I., and Östreicher, R. 1988, *A.J.*, **95**, 45.
Atwood, B., Baldwin, J. A., and Carswell, R. F. 1982, *Ap. J.*, **257**, 559.
Capriotti, E., Foltz, C., and Byard, P. 1981, *Ap. J.*, **245**, 396.
Carleton, N. P. 1985, in *Astrophysics of Active Galaxies and Quasi-stellar Objects*, ed. J. S. Miller (Mill Valley: University Science Books).
Dahari, O., and De Robertis, M. M. 1988*a*, *Ap. J. Suppl.*, **67**, 249.
———. 1988*b*, *Ap. J.*, **331**, 727.
De Robertis, M. M. 1987, *Ap. J.*, **316**, 597.
De Robertis, M. M., and Osterbrock, D. E. 1984, *Ap. J.*, **286**, 171.
———. 1986, *Ap. J.*, **301**, 98.
Filippenko, A. V. 1985, *Ap. J.*, **289**, 475.
Filippenko, A. V., and Sargent, W. L. W. 1985, *Ap. J. Suppl.*, **57**, 203.
———. 1987, *Ap. J.*, **324**, 134.
Gaskell, C. M. 1982, *Ap. J.*, **263**, 79.
Goodrich, R. W. 1989, *Ap. J.*, **340**, 190.
Heckman, T. M., Miley, G. K., van Breugel, W. J. M., and Butcher, H. R. 1981, *Ap. J.*, **247**, 403.
Krolik, J. H., and Begelman, M. C. 1988, *Ap. J.*, **329**, 702.
Krolik, J. H., and Vrtilek, J. M. 1984, *Ap. J.*, **279**, 521.
Lauer, T. R., Miller, J. S., Osborne, C. S., Robinson, L. B., and Stover, R. J. 1984, *Proc. SPIE*, **445**, 132.
Lin, D. N. C., Pringle, J. E., and Rees, M. J. 1988, *Ap. J.*, **328**, 103.
Mathews, W. G., and Veilleux, S. 1989, *Ap. J.*, **336**, 93.
Miller, J. S., and Goodrich, R. W. 1987, *Bull. AAS*, **19**, 695.
Miller, J. S., Robinson, L. B., and Schmidt, G. D. 1980, *Pub. A.S.P.*, **92**, 702.
Miller, J. S., Robinson, L. B., and Wampler, E. J. 1976, *Advances in Electronics and Physics*, Vol. **40B** (New York: Academic), p. 693.
Osterbrock, D. E. 1981, *Ap. J.*, **249**, 462.
———. 1988, *Astrophysics of Gaseous Nebulae and Active Galactic Nuclei* (Mill Valley: University Science Books).
Osterbrock, D. E., and Mathews, W. G. 1986, *Ann. Rev. Astr. Ap.*, **24**, 171.
Pelat, D., Alloin, D., and Fosbury, F. A. E. 1981, *M.N.R.A.S.*, **195**, 787.
Robinson, L. B., and Wampler, E. J. 1972, *Pub. A.S.P.*, **84**, 161.
Stone, R. P. S. 1977, *Ap. J.*, **218**, 767.
Stryker, L. L. 1987, *Nearly Normal Galaxies*, ed. S. M. Faber (New York: Springer-Verlag), p. 10.
Veilleux, S. 1989, *IAU Symposium 134, Active Galactic Nuclei*, ed. D. E. Osterbrock and J. S. Miller (Dordrecht: Kluwer), p. 312.
Vrtilek, J. M. 1985, *Ap. J.*, **294**, 121.
Vrtilek, J. M., and Carleton, N. P. 1985, *Ap. J.*, **294**, 106.
Whittle, M. 1985*a*, *M.N.R.A.S.*, **213**, 1.
———. 1985*b*, *M.N.R.A.S.*, **213**, 33.
Whittle, M., Pedlar, A., Meurs, E. J. A., Unger, S. W., Axon, D. J., and Ward, M. J. 1988, *Ap. J.*, **326**, 125.

M. M. De Robertis: Department of Physics, York University, 4700 Keele Street, North York, Ontario, Canada M3J 1P3

Richard A. Shaw: Code 684.9, NASA/Goddard Space Flight Center, Greenbelt, MD 20771